Carbon Nanotube Network Formation from Evaporating Sessile Drops

William R. Small,*,† Chris D. Walton,† Joachim Loos,‡ and Marc in het Panhuis*,†

Department of Physical Sciences, The University of Hull, Hull, HU6 7RX, UK, and Department of Chemical Engineering and Chemistry, Eindhoven University of Technology, P.O. Box 513, 5600 MB Eindhoven, The Netherlands

Received: April 17, 2006; In Final Form: May 12, 2006

Fabrication of single-walled carbon nanotube (SWNT) networks using evaporation of SDS−SWNT sessile drops on a hydrophobized silicon substrate is reported. It is suggested that the organization of nanotubes during evaporation is controlled by aggregates (in the SDS−SWNT dispersion) and hydrophobicity of the substrate. On hydrophobic substrates, the evaporation of SDS−SWNT sessile drops proceeds through constant contact area. On hydrophilic substrates, nanotube aggregates in SDS−SWNT dispersion stop the contact line from moving, resulting in the formation of "coffee-stains". The (partial) removal of aggregates by centrifugation is essential for a freely moving contact line leading to the organization of nanotubes into a network of homogeneously distributed nanotubes on the most hydrophobic substrate. The evaporation of sessile drops was characterized by microscopic, spectroscopic, and topographical techniques.

1. Introduction

Carbon nanotubes (CNTs) possess many unique electronic and mechanical properties that make them highly versatile and of great interest to researchers from a wide range of scientific disciplines.[1] One of the key challenges is processing or engineering CNTs for potential applications such as electronic components or coatings. The routes available to engineering single-walled carbon nanotubes (SWNTs) into networks with electrical and mechanical properties involve (but are not limited to) direct growth (onto a substrate)[2] and solution-based processing.[3] Nanotubes have limited solubility in organic solvents and can be "easily" dispersed in common solvents using chemical modification of the nanotubes' surface.[4] In particular, noncovalent functionalization can be advantageous over covalent functionalization as the nanotubes' unique sp^2 bonding structure is not altered. Using this type of functionalization, carbon nanotubes have been stabilized in solution using a wide range of surface-active molecules.[4,5] In particular, surfactants such as sodium dodecyl sulfate (SDS) have been studied extensively for their excellent nanotube stabilization and separation capabilities.[6] It has been proposed that SWNTs are either encapsulated in a cylindrical micelle or coated by hemimicelles, but the exact mechanism has not been conclusively established.[7,8]

It is well-known that surfactants self-assemble into ordered structures at (and beyond) the critical micelle concentration (CMC). These structures are formed to minimize the interaction between the hydrophobic part of the surfactant and the solvent. The simplest micelles are spherical, with more complex structures formed at higher concentrations.[9] The CMC for SDS (in water) is not exactly defined and is usually reported as a range: 6−8 mM (0.17−0.23% weight per volume). The self-assembly properties of surfactants can be used in organizing materials without external intervention. For example, the evaporation-induced self-assembly (EISA) process makes possible the rapid production of patterned materials (see ref 10 and references therein).

Therefore it is clear that surfactants are ideal molecules for organizing carbon nanotubes into ordered structures using a solution-based approach. This has been used to good extent in the fabrication of densely packed nanotube networks using vacuum filtration of a nanotube dispersion, resulting in so-called Buckypaper.[11,12] In a different approach, carbon nanotubes are organized by the evaporation of sessile drops (deposited from nanotube dispersions).[3,13−16] It is well-known that the evaporation of sessile drops can proceed through either constant contact *area* (and decreasing contact angle),[17,18] or by constant contact *angle* (and decreasing contact area)[19,20] as shown in Scheme 1. Examples of using the evaporation procedure to organize nanotubes include the following: fabrication of nanotube network transistors,[3] investigation of nanotube "crusting",[13] and aligning, weaving, and bending of nanotube arrays.[14−16] Alternatively, carbon nanotubes can be organized using laminar flow and controlled flocculation.[21]

In this paper, we investigate the evaporation behavior of SDS−SWNT sessile drops on a range of substrates. We found that engineering the solution−substrate contact angle provides a simple way to fabricate networks of homogeneously distributed carbon nanotubes. The sessile drops were analyzed by contact angle analysis and video microscopy. The evaporated drops (nanotube networks) were characterized using spectroscopic, microscopic, and topographical techniques.

2. Experimental Section

SWNTs produced by the high-pressure decomposition of carbon monoxide (HiPco method) were purchased from Carbon Nanotechnologies Inc., Houston, TX.[22] Nanotube dispersions were prepared by sonication of SWNTs (2 mg) in aqueous SDS (Aldrich) solutions (0.05−1.0% weight per volume) until a dense black dispersion had formed. Centrifuged solutions were prepared using an Eppendorf mini-spin centrifuge (30 min at 6000 rpm).

UV−visible spectra were recorded using a Perkin-Elmer Unicam UV3 spectrometer and normalized to the shortest wavelength UV−vis band.

* Authors to whom correspondence should be addressed. E-mail: W.Small@chem.hull.ac.uk, marc@panhuis.org.
† The University of Hull.
‡ Eindhoven University of Technology.

10.1021/jp062365x CCC: $33.50
Published on Web 06/14/2006

SCHEME 1: Schematic of the Evaporation Processes of Sessile Drops[a]

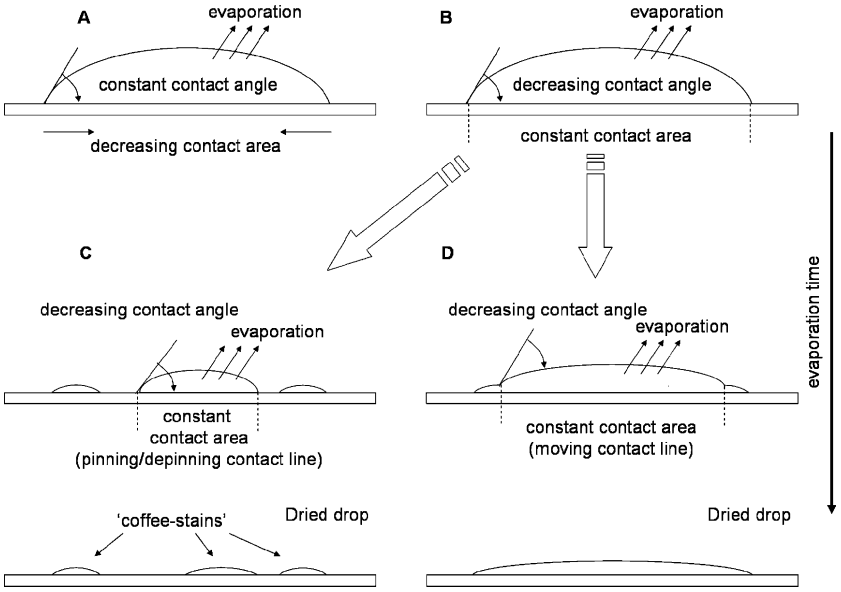

[a] (A) Constant contact angle (decreasing contact area) mechanism, (B) constant contact area (decreasing contact angle) mechanism, (C) aggregate-induced pinning and depinning leads to formation of "coffee stain deposits" at the contact line, and (D) the drop is drying via constant contact area (decreasing contact angle), and as the contact line is free to move this leads to an evenly distributed deposit.

The following substrates were used: glass microscope slides, silicon wafers, silicon wafers sputtered with a 200-nm-thick layer of copper (Texas Instruments, Richardson, TX), and silicon wafers treated with octadecyltrichlorosilane (OTS). The aim of the OTS treatment was to hydrophobize the surface of the wafer and is based on a previously reported method.[23] Briefly, the silicon wafer was submerged in a solution of 1.0% (w/v) OTS in toluene for 1 h, before being removed and washed in toluene and then ethanol (this was carried out under nitrogen and in the presence of phosphorus pentoxide). The wafers were dried overnight in an oven at 50 °C.

A Deerac Fluidics Equator single-tip liquid handling system (Equator) was used to deposit 100-nL drops onto substrates from a reservoir containing (freshly prepared) solutions or dispersions (see ref 3 for details). This allowed for noncontact deposition of sessile drops with great accuracy in the drop volume. The drops were allowed to dry in air at ambient temperature (25 °C) and relative humidity (45%).

Optical and video microscopy of evaporating drops was obtained using an Olympus BX51 optical microscope fitted with a DP50 digital camera.

Contact angle measurements were carried out in-situ on 100-nL sessile drops using the Equator augmented with a digital camera and light source (see Figure S1, Supporting Information). Images were captured every 10 s until the evaporation was complete. Contact angles were determined from the resulting images, and they represent the average of 4 sessile drops. Error analysis revealed that the uncertainty is 1−2 degrees on untreated silicon and 2−3 degrees on OTS-treated silicon.

Raman spectra were collected on evaporated drops using a Jobin Yvon Horiba high-resolution LabRam Raman inverted spectroscopic microscope spectrometer with a 632.8-nm laser excitation line.

Poly(dimethylsiloxane) (PDMS) replicas of the evaporated drops were formed from Sylgard 184 (Dow Corning) with a PDMS/cross-linker ratio of 10:1, which was degassed before pouring over the substrates. Curing occurred over 48 h at room temperature. The released replicas were stored in sealed containers to prevent surface contamination.

Topographical analysis of PDMS casts of the evaporated drops was carried out using a scanning white light interferometer (Veeco, Wyko NT1100). Surface-height information was determined from a cross-section through the deposit (evaporated drop).

Morphological investigation of evaporated drops was performed by scanning electron microscopy (XL30 ESEM-FEG, Fei Co., Eindhoven, The Netherlands). The SEM was equipped with a field emission electron source. High-vacuum conditions were applied, and a secondary electron detector was used for image acquisition. The SEM was operated either in conventional high-voltage or low-voltage mode. No additional sample treatment such as surface etching or coating with a conductive layer had been applied. Standard acquisition conditions for charge-contrast imaging were as follows: working distance of ∼5 mm for low-voltage mode and ∼10 mm for high-voltage charge-contrast imaging, spot 3, slow scan imaging with approximately 2 min/frame.

3. Results and Discussion

3.1. Surfactant Concentration. Carbon nanotubes were dispersed in aqueous SDS solutions with increasing concentration range (0.05−1.0% w/v). Stable nanotube dispersions were obtained for SDS concentrations greater than the (SDS) CMC range (0.17−0.23%). These dispersions consist of individual and bundled (aggregated) carbon nanotubes encased in surfactant. A typical UV−visible spectrum (see Figure S2, Supporting Information) is relatively featureless due to the presence of nanotube aggregates. It is well-known that nanotube aggregates can be removed using a centrifugation procedure.[6] The removal of aggregates results in more-defined peaks in the absorption spectrum due to allowed transitions between van Hove singularities. These peaks increase in intensity as the ratio of individual and aggregated nanotubes increases. The broad features in Figure S2 (Supporting Information) indicate that this ratio has been changed, leaving a relative larger proportion of individual nanotubes in solution.

Drops of aqueous SDS solutions (100 nL) over the concentration range 0.05−1.00% (w/v) SDS were deposited onto un-

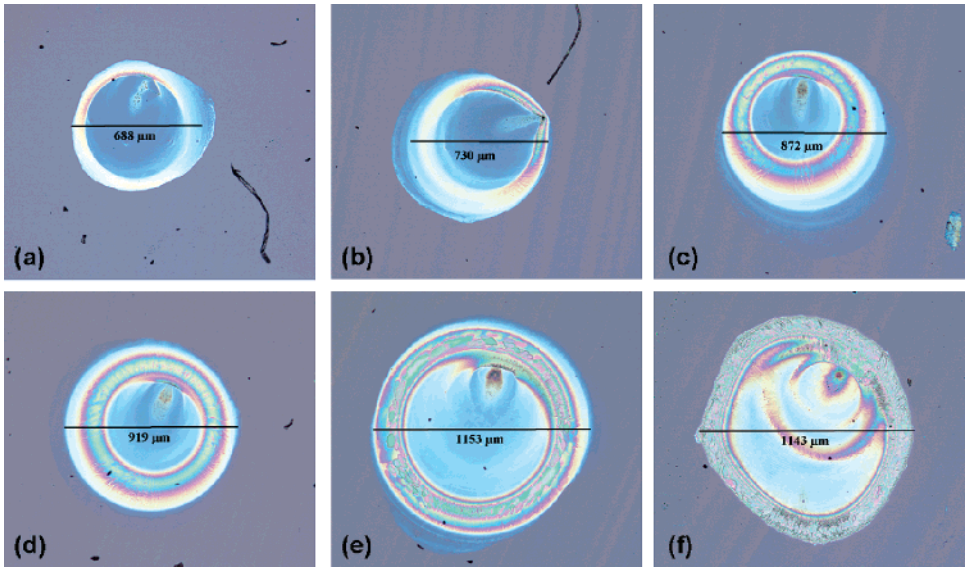

Figure 1. Optical microscopy images of evaporated drops deposited from 100-nL SDS solutions on untreated silicon at concentrations (in weight per volume): (a) 0.05%, (b) 0.10%, (c) 0.20%, (d) 0.25%, (e) 0.50%, and (f) 1.00%.

treated silicon substrates using a liquid handling system and allowed to dry (Figure 1). The film diameter increases with increasing surfactant concentration. This is in excellent agreement with the increased wetting of the substrate due to decreasing surface tension. In addition, enhanced structural features are observed for concentration above the CMC range (Figure S3, Supporting Information).

These features include linear striations forming perpendicular to the film circumference and liquid-crystal-type structures at the perimeter of the film (Figure S3, Supporting Information); these are in agreement with previously observed SDS self-assembly features.[24]

The minimum amount of SDS necessary to cover the maximum available SWNT surface area can be estimated as follows. The surface area (A_{CNT}) of 1 g of homogeneously dispersed individual SWNTs is approximately 1500 m^2. To cover this completely with SDS molecules (assuming the SDS ideal surface area, $A_{SDS} = 0.57$ nm^2) requires 1.3 g of SDS.

On the basis of these observations, all further work is carried out at a SDS concentration of 0.25% weight per volume because (1) this allows formation of stable CNT dispersions, (2) it enables self-assembly features, that is, above the CMC range, (3) it provides excess SDS surface area compared to available CNT surface area (at this concentration), and (4) SDS concentration is not too high to impede electron microscopy.

3.2. Centrifugation. Drops (100-nL) of aqueous SDS solution and as-prepared and centrifuged SDS−SWNT dispersions were deposited onto an untreated silicon substrate and followed over time (see Figure S4, Supporting Information). The evaporated drop from an as-prepared SDS−SWNT dispersion exhibits a series of circular ring-like deposits, similar to so-called "coffee-stains".[17] These rings all pass through one part of the outer "coffee-stain", giving the deposit a lopsided and unsymmetrical appearance. In contrast to this, the deposit formed following evaporation of a drop deposited from a centrifuged dispersion exhibits linear striations and liquid-crystal-type features similar to those observed for SDS solutions at higher concentrations (see Figure S3, Supporting Information). However, it is clear from the images that evaporation of drops deposited from SDS solutions and centrifuged SDS−SWNT dispersions result in evaporated deposits which are significantly smaller compared to the initial size of the sessile drop (immediately after deposition).

Thus, it is obvious that centrifugation of the nanotube dispersion has a significant effect on the evaporation behavior of the sessile drop. This is reflected in the difference in the mean contact angle and baseline diameter during evaporation (see Figures S5 and S6, Supporting Information).

Sessile drops from centrifuged dispersions show different evaporation behavior. The baseline diameter steadily decreases, while the contact angle increases slightly until all solvent had evaporated (see Figure S6, Supporting Information). This behavior is consistent with evaporation via decreasing contact area (see Scheme 1) and similar to that observed for evaporating sessile drops from SDS solutions.

3.3. Substrate Hydrophobicity. Let us now further address these observations and investigate the role of substrate hydrophobicity on evaporated drop formation and morphology. Figure 2 shows drops deposited from solutions (SDS) and dispersions (SWNT−SDS) onto substrates with an increasing degree of hydrophobicity (indicated by substrate−liquid contact angle, see Table 1). As expected, the area covered by sessile drops decreases with increasing (substrate−liquid) contact angle. The (evaporated) drops from centrifuged dispersions are similar in size to those formed from as-prepared dispersions only on copper and OTS-treated silicon substrates. The deposits from as-prepared dispersions show "coffee-stains" around the edge.

3.4. Evaporation Behavior. Information about changes in contact angle and baseline diameter can provide insight into the evaporation behavior of sessile drops. An example of contact angle analysis for a drop from a centrifuged dispersion on OTS-treated silicon substrate is shown in Figure 3. The contact angle steadily decreases whereas the baseline diameter remains constant until the final stage of evaporation (Scheme 1B). During this (final) stage the contact angle levels off at around 7°, while the baseline diameter recedes until all of the solution has evaporated (Scheme 1D). This final stage is referred to as film (dried drop) formation.

Figure 4 shows the baseline diameters of evaporating drops (from centrifuged SDS−SWNT dispersions) on different substrates. The evaporation time increases with increasing substrate hydrophobicity. On the most hydrophobic substrates, the evaporation process proceeds through constant contact area

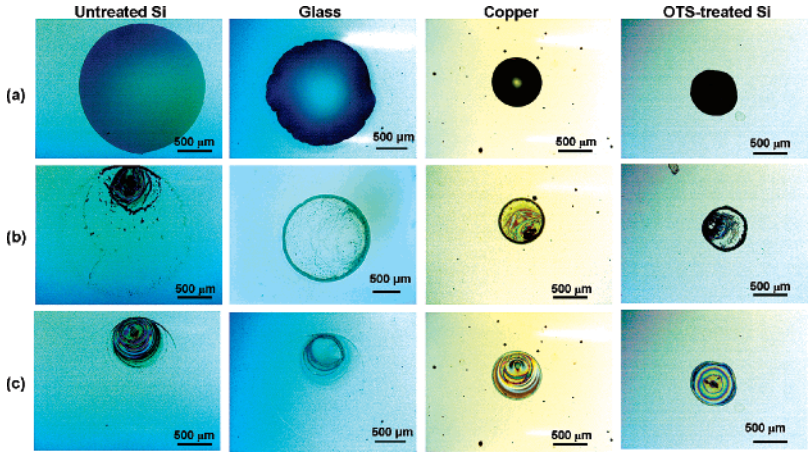

Figure 2. Optical microscopy images of 100-nL drops deposited from 0.25% (w/v) SDS−SWNT dispersions on substrates with increasing hydrophobicity. (a) Immediately after deposition, (b) evaporated drops from as-prepared dispersions, and (c) evaporated drops from centrifuged dispersions.

TABLE 1: Initial Substrate−Liquid Contact Angles and Baseline Diameters for 100-nL Drops Deposited from a Centrifuged 0.25% (w/v) SDS−SWNT Dispersion

substrate	baseline diameter (mm)	substrate−liquid contact angle (degrees)
untreated silicon	2.20	3
glass slide	1.80	8
copper-sputtered silicon wafer	0.87	50
OTS-treated silicon	0.79	80

(Scheme 1B) until the final stage of evaporation (indicated by arrows). During the final stage the contact line moves until all solvent has evaporated (Scheme 1D). On glass slides, the evaporation process initially proceeds through constant contact area (for about 30 s) before changing to decreasing contact area. While on the least hydrophobic substrate (untreated silicon), the evaporation proceeds via decreasing contact area (Scheme 1A).

The contact angles at the start of film formation can be calculated from interference fringes (see Figure S7, Supporting Information) observed during the final stage of evaporation. These interference fringes at the edge of the drops (an effect similar to "Newton's rings") are used to determine the contact angle of the drop.[25] These occur due to periodic constructive and destructive interference of the incident light, caused by the thinness of the film.[26] Line-profiles giving the light intensity as a function of distance perpendicular to the contact line can be obtained using image analysis software (Figure S7, Supporting Information). The contact angle (θ) during film formation can be calculated using $\theta = \tan^{-1}(i\lambda/2ns)$, where i is the fringe number (an integer), λ is the wavelength of the incident light, n is the refractive index, and s is the distance between fringes. For simplification, a number of assumptions are made: (i) the refractive index of the solution has not been altered by the presence of surfactant or nanotubes and is equal to that of water, and (ii) the incident light is monochromatic ($\lambda = 406$ nm), normal to the substrate with no stray light. Under these assumptions, contact angles of $3.6° \pm 1.3°$ (on untreated silicon) and $3.2° \pm 1.1°$ (on OTS-treated silicon) are obtained. These values are in good agreement with contact angle analysis measurements (see Figure 3 and also Figure S6 of Supporting Information).

The appearance of symmetric features in the film depends on the movement of the contact line during the film-forming process and is governed by the hydrophobicity of the substrate (see Figure 5). On a hydrophilic substrate (untreated silicon), the contact line is pinned (at the top of this drop) during film formation and does not recede equally, leading to the lopsided appearance (Figure 5a and Scheme 1C). In contrast, on a hydrophobic substrate (OTS-treated silicon) the contact line clearly recedes equally from all around the drop (i.e., no pinning), resulting in a concentric (and symmetric) ring formation (see Scheme 1D). Hence, the substrate hydrophobicity plays an important role in the appearance of the evaporated (dried) drop.

3.5. Nanotube Distribution. The distribution of nanotubes in the films was investigated using Raman spectroscopy (for detection) and SEM (for visualization). It is well-known that the Raman spectrum of HiPco SWNTs exhibits distinctive features.[27] One of these features, the so-called G-band ($\sim$1600 cm^{-1}) is used for probing the distribution of nanotubes in the evaporated drop (not shown).

In deposits formed after evaporation of an as-prepared dispersion, Raman spectroscopy suggests that the nanotubes are predominantly concentrated in the "coffee-stains" and are not homogeneously distributed over the entire film (and hence cannot be organized into a network). However, Raman spectroscopy on thin films formed from centrifuged dispersions showed that nanotubes are homogeneously distributed over the entire film area, in particular on OTS-treated silicon.

Scanning electron microscopy confirmed these Raman observations. The "coffee-stains" (in thin films from as-prepared dispersions) consist of nanotube aggregates organized in a random fashion not dissimilar to a plate of "spaghetti" (Figure 6A).

The deposit formed after evaporation of a centrifuged dispersion is dominated by the linear striations associated with SDS (see Figure S3, Supporting Information). Conventional SEM (Figure 6B) reveals merely the surface of the sample, which is dominated by these surfactant features. The "holes" visible in the film are an artifact introduced by local heating of the sample by the electron beam during imaging, as are the nanotubes bridging these features. Figure 6, parts C and D, show SEM images acquired for low-voltage and charge-contrast conditions, respectively. For a low acceleration voltage of 1 kV, merely the surface of the sample can be investigated, indicating the presence of nanotubes at or near the deposit surface. In contrast, application of charge-contrast imaging of the same sample area allows for visualization of nanotubes embedded deeper in the deposit.[28] Charge-contrast images

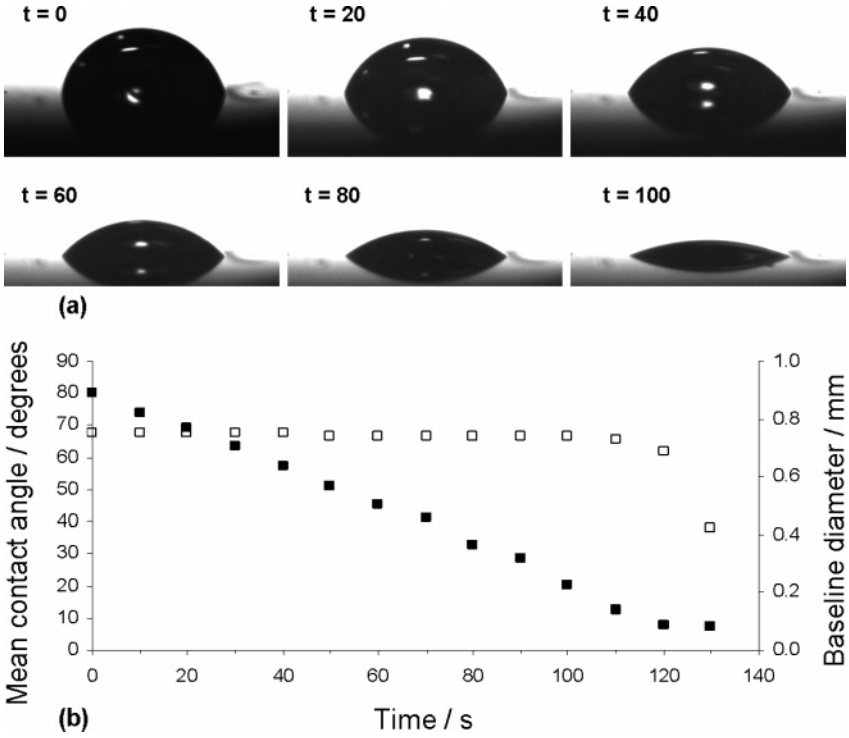

Figure 3. (a) Images used in the contact angle analysis of a 100-nL drop, deposited from a centrifuged 0.25% (w/v) SDS−SWNT dispersion, on OTS-treated silicon substrate. Times above images refer to the time after drop deposition. (b) Mean contact angle (filled squares) and baseline diameter (empty squares) as determined by contact angle analysis.

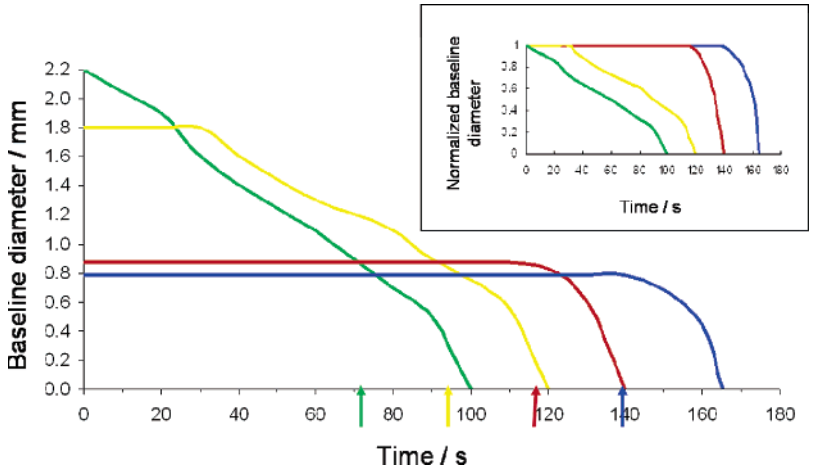

Figure 4. Baseline diameters as a function of time for 100-nL drops (deposited from a centrifuged 0.25% (w/v) SDS−SWNT dispersion), on substrates with increasing hydrophobicity; untreated silicon (green line), glass slide (yellow line), copper-sputtered silicon wafer (red line), and OTS-treated silicon (blue line). Arrows indicate the final stage in the evaporation process. Inset: data normalized to initial baseline diameter (at $t = 0$ s).

showed that nanotubes are homogeneously distributed throughout the deposit and have organized (self-assembled) into a network.

3.6. Topographical Analysis. Determining the height of the evaporated drops was extremely difficult using direct measurements due to the complex refractive index of these deposits. To avoid this problem, PDMS was used to replicate evaporated drops before carrying out topographical analysis. PDMS has previously been used to replicate features as small as 2 nm.[29] Using a replica requires inversion of the graphical profile necessary to show drop features the correct way up. The graphical profiles obtained by inversion of the data from a single PDMS replica were in excellent agreement with data from a double PDMS replica (see Figures S8 and S9, Supporting Information). It was observed that topographical analysis provides insights into the thickness and surface profiles of evaporated drops. For example, analysis of a deposit after evaporation of an as-prepared SDS−SWNT dispersion on OTS-treated silicon provides additional evidence for the "coffee-stains" observed in optical microscopy (see Figure S10, Supporting Information). In particular, the height profile of the deposit from an as-prepared dispersion shows irregular features indicative of the asymmetrical nature of the film.

The difference in features ("coffee-stains", concentric rings) observed using optical microscopy (see Figure 5) for evaporated drops from centrifuged dispersions is confirmed by topographical analysis. The irregular features for an evaporated drop on untreated silicon are clearly visible in the topographical images (Figure 7). In particular, height analysis confirms that the drop features are asymmetric, with thickness varying from negligible

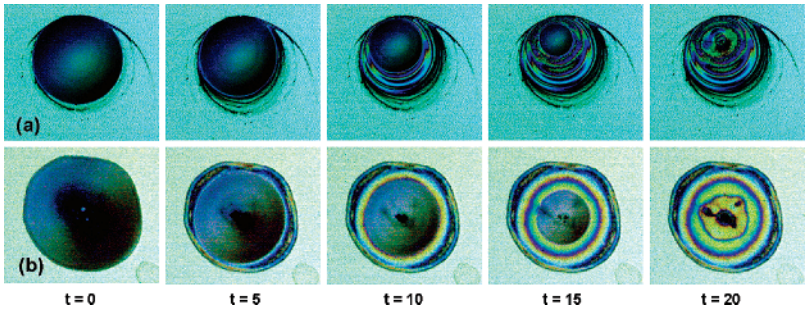

Figure 5. Video microscopy images of 100-nL drops (deposited from a centrifuged 0.25% (w/v) SDS−SWNT dispersion) on (a) untreated silicon, and (b) OTS-treated silicon substrates. $t = 0$ indicates the onset of the final stage in the evaporation process.

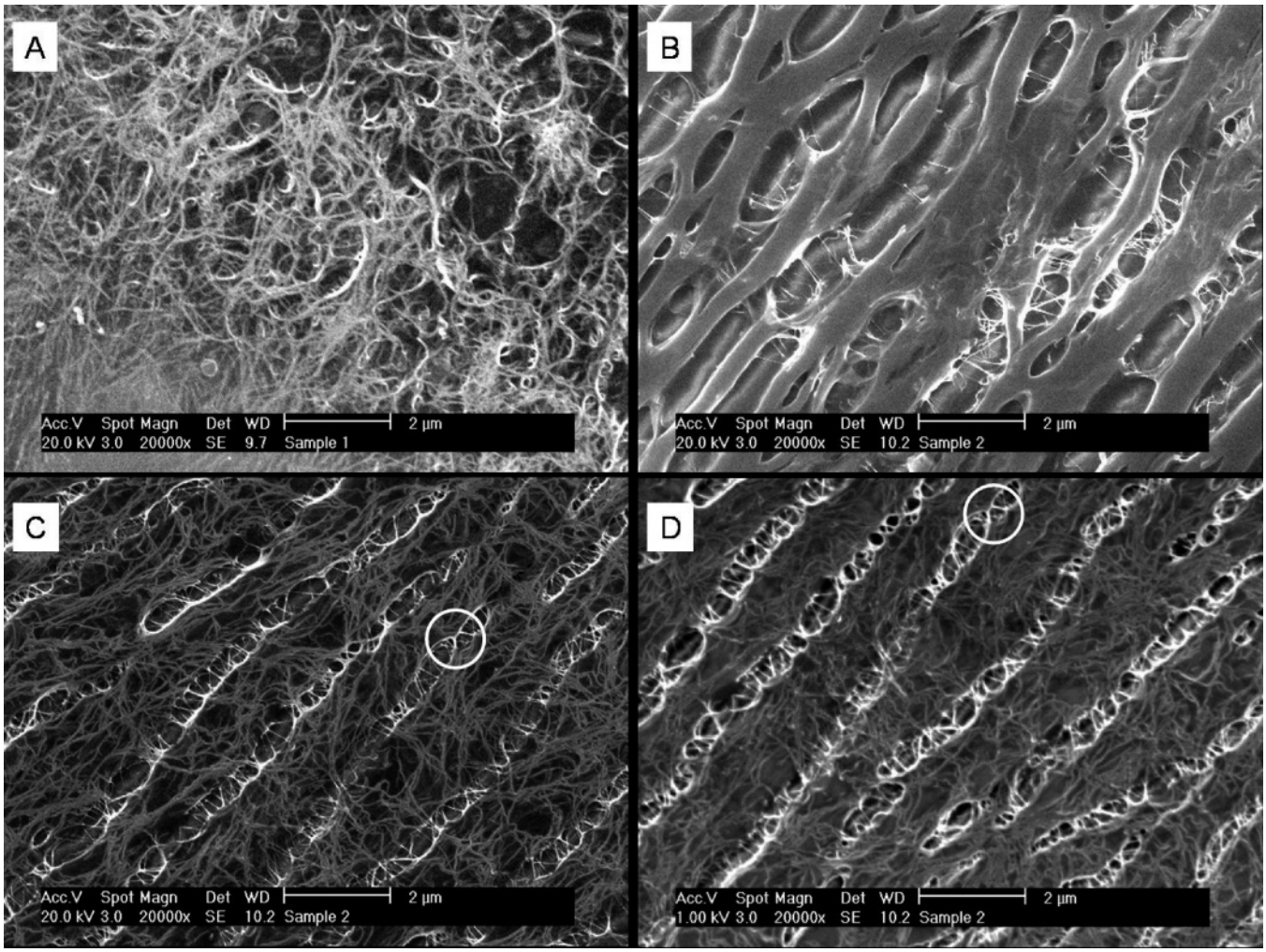

Figure 6. Scanning electron microscopy (SEM) images of (A) "coffee-stain" area in an evaporated drop from an as-prepared SDS−SWNT dispersion, and (B) typical area in an evaporated drop from a centrifuged SDS−SWNT dispersion. SEM charge-contrast images acquired at acceleration voltages of 20 kV (C) and 1 kV (D). Circle indicates reference point.

to 1 μm, while topographical analysis of an evaporated drop on the most hydrophobic substrate confirms the symmetrical nature of the deposit (see Figure 8). Height profile analysis clearly shows the symmetry with thickness of the deposit between 300 and 600 nm.

3.7. Network Composition. The height profile data (from topographical analysis) can be used to provide a qualitative measure for evaporated drop volume through the area under the curve (A_{film}). This yields 180, 200, and 140 μm^2 for evaporated drops deposited from SDS solution, as-prepared SDS−SWNT dispersion, and centrifuged SDS−SWNT dispersion, respectively. These relative values are in good agreement with the (estimated) amount of material in each 100-nL drop (assuming homogeneous solutions/dispersions). A 100-nL drop of 0.25% SDS solution contains 250 ng of SDS, whereas a 100-nL drop of 0.25% SDS−SWNT contains 250 ng of SDS and 33 ng of SWNT. The calculated mass per area is similar for both films ($\sim$1.4 ng/μm^2). Assuming a similar mass per area for the drop from the centrifuged dispersion allows for an estimate of 196 ng of material (SDS + SWNT), suggesting a loss of 87 ng of material during centrifugation. This corresponds to a SDS concentration ranging between 0.15% (no removal of nanotube material) and 0.20% (removal of all nanotube material).

An estimate for the electrical conductivity was obtained by measuring the resistance across the network (using conductive

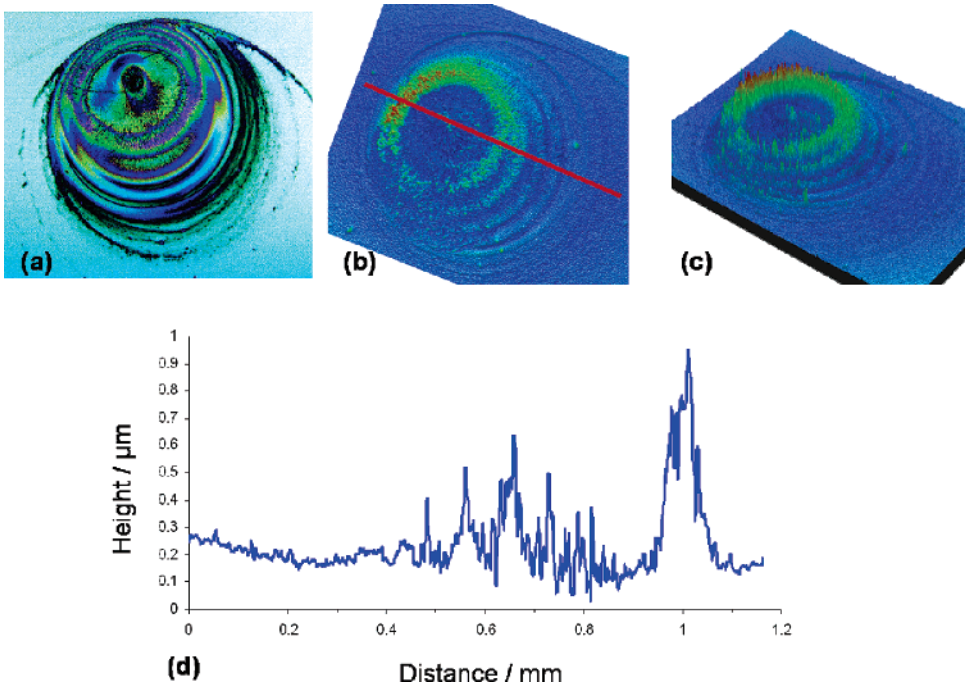

Figure 7. (a) Optical microscopy image of an evaporated drop (deposited from a centrifuged 0.25% (w/v) SDS−SWNT dispersion) on untreated silicon. Corresponding topographical analysis on PDMS replica: (b) 2D view in same orientation as optical image, (c) 3D view, and (d) height profile (obtained over red line) as a function of drop diameter.

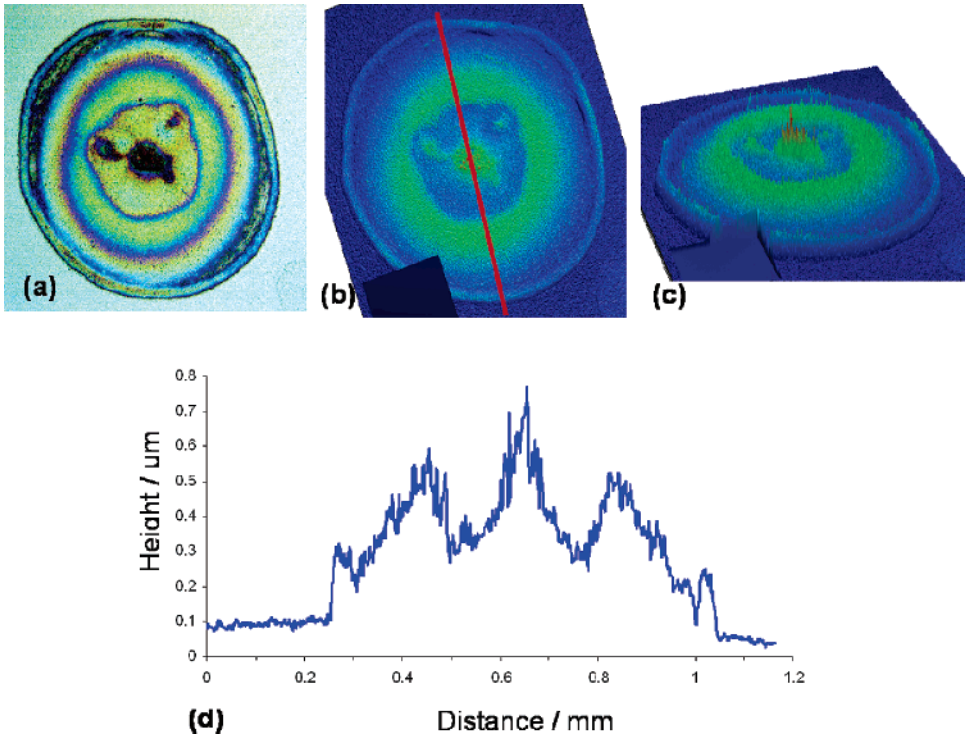

Figure 8. (a) Optical microscopy image of an evaporated drop (deposited from a centrifuged 0.25% (w/v) SDS−SWNT dispersion) on OTS-treated silicon. Corresponding topographical analysis on PDMS replica: (b) 2D view in same orientation as optical image, (c) 3D view, and (d) height profile (obtained over red line) as a function of drop diameter.

paint for making contacts). The electrical resistance of nanotube networks on OTS-treated silicon was approximately 50 ± 2 kΩ, yielding an electrical conductivity of $\sim 2 \times 10^{-5}$ S/sq. The conductivity of a material is calculated from $\sigma = l/RA$, where A is the film area, and l is the distance over which the resistance R is obtained. Estimating the film area from the area under the curve (in Figure 8) yields a conductivity of approximately 100 S/m. Further work involving an investigation of the transport properties is necessary to fully understand the electronic properties of these networks.

4. Discussion

In this work the following two factors have been investigated for their effect on the organization of carbon nanotubes into a network (of homogeneously distributed nanotubes): centrifugation of the dispersion and hydrophobicity of the substrate.

Evaporation of sessile drops from as-prepared dispersions resulted in an inhomogeneous distribution of carbon nanotubes on *all* substrates due to aggregate-induced pinning of the contact line. The aggregates stop the contact line from moving, resulting in a constant contact area (and decreasing contact angle). Because of a gradient in the evaporation rate over the drop surface, an outward flow of solution from the center of the drop to the contact line occurs (as observed by video microscopy). This flow carries aggregates to the contact line leading to the formation of a "coffee-stain" deposit (see Scheme 1C).

Evaporation of sessile drops from centrifuged dispersions resulted in a homogeneous distribution of carbon nanotubes on the most hydrophobic substrate (OTS-treated silicon). The mechanism of evaporation is via constant contact area (and decreasing contact angle). As the contact line is free to move (due to absence of aggregate-induced pinning), pinning does not occur; this results in formation of nanotubes organized into a network (see Scheme 1D).

Thus it is obvious that evaporation of an aggregate-free dispersion proceeding via constant contact area is crucial to the formation of a network consisting of homogeneously distributed nanotubes.

5. Conclusion

In summary, we have investigated the evaporation behavior of SDS−SWNT sessile drops on a range of substrates. We found that engineering the solution−substrate contact angle provides a simple way to fabricate networks of homogeneously distributed carbon nanotubes. This aids the development of processing SWNT materials into coatings or electronic components.

Acknowledgment. We gratefully acknowledge financial support from EPSRC, The Royal Society, and Science Research Investment Fund (SRIF). Dr. X. Zhang and Prof. S. J. Haswell are thanked for their assistance with Raman spectroscopy.

Supporting Information Available: Schematic of setup for contact angle analysis, UV−visible absorption spectra, optical and video microscopy images, contact angle data, interference data, topographical analysis, and photographs. This material is available free of charge via the Internet at http://pubs.acs.org.

References and Notes

(1) Baughman, R. H.; Zakhidov, A. A.; de Heer, W. A. *Science* **2002**, *297*, 787−792.

(2) Bradley, K.; Gabriel, J.-P. C.; Grüner, G. *Nano Lett.* **2003**, *3*, 1353−1355.

(3) in het Panhuis, M.; Gowrisanker, S.; Vanesko, D. J.; Mire, C. A.; Jia, H.; Xie, H.; Baughman, R. H.; Musselman, I. H.; Gnade, B. E.; Dieckmann, G. R.; Draper, R. K. *Small* **2005**, *1*, 820−823.

(4) Tasis, D.; Tagmatarchis, N.; Bianco, A.; Prato, M. *Chem. Rev.* **2006**, *106*, 1105−1136.

(5) Lin, Y.; Taylor, S.; Li, H.; Fernando, K. A. S.; Qu, L.; Wang, W.; Gu, L.; Zhou, B.; Sun, Y.-P. *J. Mater. Chem.* **2004**, *14*, 527−541.

(6) O'Connell, M. J.; Bachilo, S. M.; Huffman, C. B.; Moore, V. C.; Strano, M. S.; Haroz, E. H.; Rialon, K. L.; Boul, P. J.; Noon, W. H.; Kittrell, C.; Ma, J.; Hauge, R. H.; Weisman, R. B.; Smalley, R. E. *Science* **2002**, *297*, 593−596.

(7) Richard, C.; Balavoine, F.; Schultz, P.; Ebbesen, T. W.; Mioskowski, C. *Science* **2003**, *300*, 775−778.

(8) Yurekli, K.; Mitchell, C. A.; Krishnamoorti, R. *J. Am. Chem. Soc.* **2004**, *126*, 9902−9903.

(9) Israelachvili, J. N. *Intermolecular and Surface Forces: With Applications to Colloidal and Biological Systems*; Academic Press: London, 1985.

(10) Brinker, C. J.; Lu, Y.; Sellinger, A.; Fan, H. *Adv. Mater.* **1999**, *11*, 579−585.

(11) Frizzell, C. J.; in het Panhuis, M.; Coutinho, D. H.; Balkus, K. J., Jr.; Minett, A. I.; Blau, W. J.; Coleman, J. N. *Phys. Rev. B* **2005**, *72*, 245420.

(12) Dettlaff-Weglikowska, U.; Skakalova, V.; Graupner, R.; Jhang, S. H.; Kim, B. H.; Lee, H. J.; Ley, L.; Park, Y. W.; Berber, S.; Tomanek, D.; Roth, S. *J. Am. Chem. Soc.* **2005**, *127*, 5125−5131.

(13) Duggal, R.; Hussain, F.; Pasquali, M. *Adv. Mater.* **2006**, *18*, 29−34.

(14) Huang, L.; Cui, X.; Dukovic, G.; O'Brien, S. P. *Nanotechnology* **2004**, *15*, 1450−1454.

(15) Ko, H.; Peleshanko, S.; Tsukruk, V. V. *J. Phys. Chem. B* **2004**, *108*, 4385−4393.

(16) Tsukruk, V. V.; Ko, H.; Peleshanko, S. *Phys. Rev. Lett.* **2004**, *92*, 065502.

(17) Deegan, R. D.; Bakajin, O.; Dupont, T. F.; Huber, G.; Nagel, S. R.; Witten, T. A. *Nature* **1997**, *389*, 827−829.

(18) Deegan, R. D. *Phys. Rev. E* **2000**, *61*, 475−485.

(19) Picknett, R. G.; Bexon, R. *J. Colloid Interface Sci.* **1997**, *61*, 336−350.

(20) Hu, H.; Larson, R. G. *J. Phys. Chem. B* **2002**, *106*, 1334−1344.

(21) Park, J. U.; Meitl, M. A.; Hur, S. H.; Usrey, M. L.; Strano, M. S.; Kenis, P. J. A.; Rogers, J. A. *Angew. Chem., Int. Ed.* **2006**, *45*, 581−585.

(22) Nikolaev, P.; Bronikowski, M.; Bradley, R.; Roymund, F.; Colbert, D.; Smith, K.; Smalley, R. E. *Chem. Phys. Lett.* **1999**, *313*, 91−97.

(23) Cayre, O. J.; Paunov, V. N. *Langmuir* **2004**, *20*, 9594−9599.

(24) Kékicheff, P.; Grabielle-Madelmont, C.; Ollivon, M. *J. Colloid Interface Sci.* **1989**, *131*, 122−132.

(25) Stöckelhuber, K. W.; Radoev, B.; Schulze, H. J. *Colloids Surf., A* **1999**, *156*, 323−333.

(26) Middleton, L. R. *A Textbook of Light*; G. Bell and Sons, Ltd.: London, 1958.

(27) Chambers, G.; Carroll, C.; Farrell, G. F.; Dalton, A. B.; McNamara, M.; Cummins, E.; in het Panhuis, M.; Byrne, H. J. *Nano Lett.* **2003**, *3*, 843−846.

(28) Loos, J.; Alexeev, A.; Grossiord, N.; Koning, C. E.; Regev, O. *Ultramicroscopy* **2005**, *104*, 160−167.

(29) Hua, F.; Sum, Y.; Gaur, A.; Meitl, M. A.; Bilhaut, L.; Rotkina, L.; Wang, J.; Geil, P.; Shim, M.; Rogers, J. A. *Nano Lett.* **2004**, *4*, 2467−2471.